



Excitation function and isomeric ratio of Tc-isotopes from the $^{93}\text{Nb}(\alpha, xn)$ reaction

K. Kim ^a, G.N. Kim ^{a,*}, H. Naik ^{a,c}, M. Zaman ^a, S.-C. Yang ^b, T.-Y. Song ^b,
R. Guin ^d, S.K. Das ^d

^a Department of Physics, Kyungpook National University, Daegu 702-701, Republic of Korea

^b Nuclear Data Center, Korea Atomic Energy Research Institute, Daejeon 305-353, Republic of Korea

^c Radiochemistry Division, Bhabha Atomic Research Center, Trombay, Mumbai 400085, India

^d Variable Energy Cyclotron Centre, 1/AF Bidhan Nagar, Kolkata 700064, India

Received 29 September 2014; received in revised form 20 December 2014; accepted 22 December 2014

Available online 5 January 2015

Abstract

The excitation functions of $^{94-96}\text{Tc}$ isotopes and independent isomeric ratios of $^{93\text{m},g}\text{Tc}$, $^{94\text{m},g}\text{Tc}$, and $^{95\text{m},g}\text{Tc}$ from the $^{93}\text{Nb}(\alpha, xn)$ reaction within the energy range below 40 MeV have been determined by using a stacked-foil activation and an off-line γ -ray spectrometric technique at the Variable Energy Cyclotron Center, Kolkata, India. The excitation function of $^{94-96}\text{Tc}$ in the $^{93}\text{Nb}(\alpha, xn)$ reaction was also calculated by using the computer code TALYS 1.6. The present data are found to be in general agreement with the literature data but have similar trend with some deviation from calculated data of the TALYS 1.6 code. The isomeric ratios of $^{93\text{m},g}\text{Tc}$, $^{94\text{m},g}\text{Tc}$, and $^{95\text{m},g}\text{Tc}$ in the $^{93}\text{Nb}(\alpha, xn)$ reactions from the present work and literature data were compared with similar data in the $^{93}\text{Nb}(^3\text{He}, xn)$ and $^{96}\text{Mo}(p, xn)$ reactions. In all the three reactions, the isomeric ratios increase with the increasing excitation energy. However, at all excitation energies, the isomeric ratios of $^{93\text{m},g}\text{Tc}$, $^{94\text{m},g}\text{Tc}$, and $^{95\text{m},g}\text{Tc}$ in the $^{93}\text{Nb}(\alpha, xn)$ and $^{93}\text{Nb}(^3\text{He}, xn)$ reactions are higher than those in the $^{96}\text{Mo}(p, xn)$ reactions, which indicate the role of input angular momentum besides excitation energy. Above the excitation energy of 35–55 MeV, the isomeric ratios of $^{95\text{m},g}\text{Tc}$, $^{94\text{m},g}\text{Tc}$, and $^{93\text{m},g}\text{Tc}$ decrease in all the $^{93}\text{Nb}(\alpha, xn)$, $^{93}\text{Nb}(^3\text{He}, xn)$ and $^{96}\text{Mo}(p, xn)$ reactions. This decreasing trend at higher excitation energy indicates the starting of pre-equilibrium reaction, which depends on the target, projectile, and type of reaction products.

© 2015 Elsevier B.V. All rights reserved.

* Corresponding author. Tel.: +82 53905320; fax: +82 539393972.

E-mail address: gnkim@knu.ac.kr (G.N. Kim).

Keywords: Excitation functions of $^{94-96}\text{Tc}$; Isomeric ratios of $^{93\text{m},\text{g}}\text{Tc}$, $^{94\text{m},\text{g}}\text{Tc}$, and $^{95\text{m},\text{g}}\text{Tc}$; $^{93}\text{Nb}(\alpha, xn)$ reaction; Stacked-foil activation technique, off-line γ -ray spectrometric technique, entrance channel parameters

1. Introduction

Experimental investigation on charged particle induced reaction cross-sections is important for nuclear data application in various fields because these reactions are used in medical and industrial applications, accelerator and nuclear technology, and to test the theoretical model. In particular, the reaction cross-section of metastable- and ground-state of the reaction products are needed for the determination of isomeric cross section ratio or isomeric ratio (IR) of the reactions products. The isomeric ratio gives an idea about the level density and discrete level structure of the residual nucleus [1,2]. The IR of reaction products in different reactions also provides information about the effect of entrance channel parameters such as excitation energy and input angular momentum [3,4]. Besides this, it gives idea about the reaction mechanism such as compound [1,2] and pre-compound process [5].

The charged particle induced reaction cross-sections and isomeric ratios for various products are available in different evaluations [6–9] and EXFOR compilation [10]. In particular, sufficient reaction cross-sections and isomeric ratios for the Tc-isotopes in the charged particle induced reactions are available in literature [11–39]. The cross-sections and the isomeric ratios of Tc-isotopes from the $^{93}\text{Nb}(\alpha, xn)$ reaction [11–30] were measured to explain the compound and non-compound (pre-equilibrium) process. On the other hand, the $^{\text{nat}}\text{Mo}(p, xn)$ reactions [34–39] are concentrated on either for the cross-section measurements or to examine the byproducts cross-section during the feasibility of ^{99}Mo – $^{99\text{m}}\text{Tc}$ production from the medical point of view [33]. The isomeric yield ratios of different Tc isotopes were also obtained during the measurement of cross-section. Branquinho et al. [15] obtained the isomeric ratios of ^{93}Tc , ^{94}Tc , ^{95}Tc , and ^{96}Tc at various alpha energies from the $^{93}\text{Nb}(\alpha, xn)$ reaction and examine the effect of pre-equilibrium reaction. Similarly, the pre-equilibrium reaction was also explained by Agrawal et al. [26], Mukherjee et al. [27], and Sharma et al. [28] based on the isomeric ratios of $^{95\text{m},\text{g}}\text{Tc}$ and $^{96\text{m},\text{g}}\text{Tc}$ from the $^{93}\text{Nb}(\alpha, xn)$ reaction. However, from the isomeric ratios of Tc-isotopes [11–30], the reaction mechanism with particular reference to the effect of entrance channel parameters such as effect of excitation energy and input angular momentum have been not explained. On the other hand, in the d- and He-induced pre-equilibrium decay, the effect of entrance and exit channel phenomena has clearly shown by Bissem et al. [40].

In view of the above fact, we measured the reaction cross-sections of $^{94-96}\text{Tc}$ and isomeric ratios of $^{93-95}\text{Tc}$ isomeric pairs from the $^{93}\text{Nb}(\alpha, xn)$ reaction within the alpha energies of 9–39 MeV by using a stacked-foil activation and an off-line γ -ray spectrometric technique. The measurements of cross-section and isomeric ratios of $^{93-96}\text{Tc}$ isomeric pairs from the $^{93}\text{Nb}(\alpha, xn)$ reaction were chosen because so many isotopes of Tc have isomeric states with suitable half-lives. The excitation functions of $^{94-96}\text{Tc}$ in the $^{93}\text{Nb}(\alpha, xn)$ reaction were also calculated by using the computer code TALYS 1.6 [41] and compared with the experimental data of the present work and literature data [24–29]. On the other hand, the isomeric ratios of $^{93-95}\text{Tc}$ isomeric pairs in the $^{93}\text{Nb}(\alpha, xn)$ reaction from the present work and literature data are compared with the similar data in the $^{93}\text{Nb}(\alpha, xn)$ [32] and $^{96}\text{Mo}(p, xn)$ [31] reactions to examine the effect of excitation energy and input angular momentum.

2. Experimental details

The experiment was carried out using the cyclotron at Variable Energy Cyclotron Centre (VECC), Kolkata, India [26–28]. The conventional stack-foil activation technique was used in the experiment as done by most of the authors [15–30]. The size of the high-purity (> 99.999%) Nb foil was 1 cm × 1 cm with thickness of 17.5 μm. 10 μm thick natural copper (> 99.98% purity) and 25 μm thick natural aluminum (> 99.999% purity) foils with the same size of 1 cm × 1 cm with known cross-sections were also used in the stacks as a beam flux monitor and an energy degrader. We made two stack-foils in order to measure cross-sections for different input alpha energies. The first stack consists of eight sets of Nb–Cu foils and one Nb foil at the end of stack. The second stack was made by adding a 25-μm thick Al foil in front of the first stack without the last Nb foil. This additional Al foil was used as an energy degrader to reduce the input alpha energy in each foil. All these foils were stacked together for the irradiation in an aluminum holder having a hole of 1.2 cm diameter in its center. The eight Cu foils having known $\text{Cu}(\alpha, x)^{66, 67}\text{Ga}$ reaction cross-sections [42] were used as the alpha beam flux monitor from 8.86 to 39.25 MeV as well as energy degrader in the higher energy side.

One of the stacked-foils was irradiated for 45 minutes with a 40 MeV diffused alpha beam of diameter 8 mm and beam current of about 120 nA in the external beam line of the cyclotron at VECC, Kolkata [26–28]. The other set of stack-foils was irradiated for 1.5 hours with a 40 MeV alpha beam of 60 nA beam current. The beam current was monitored from a current integrator of the electron suppressed Faraday cup installed behind the target-catcher assembly. The beam intensity was kept constant during the irradiation. It was necessary to ensure that equal areas of the monitor and the target foils intercepted the beam. The beam energy was determined from a curve that related to the cyclotron RF with energy constructed from experimental data on elastic scattering. The irradiation geometry was kept in a position so that the targets and monitor foils received the same beam intensity.

The irradiated target assembly was cooled for one hour and opened after measuring the dose. The irradiated Nb and Cu samples were mounted on different Perspex plate for the γ -ray counting. The γ -ray activities of the radioisotopes produced from the target and the monitor foils were measured by using a 100 cm³ HPGe detector coupled to a PC-based 4096 channel analyzer. The efficiency and energy calibration was done using the standard γ -ray sources of ¹³³Ba and ¹⁵²Eu. The resolution of the detector system was 2.0 keV at 1332.5 keV of ⁶⁰Co. The source-to-detector distance was kept long enough to assure a point-like geometry and a low dead time. In the first set of measurements, the distances between the sample and the detector was kept 25 cm to keep dead time less than 10% and to suppress the sum-coincidence effect. The γ -ray measurements of the irradiated samples were started from the lowest alpha energy side after one hour of cooling time, due to the high radiation dose of the short-lived reaction products. The γ -ray counts of other samples were also done one after another from the low-energy to the high-energy alpha irradiated samples. Special care was taken to complete decay of shorter-lived parent nuclides in the measurements of cross-sections for cumulative formation of the corresponding longer-lived daughter nuclides. Each sample was counted 3–4 times with increasing counting time to avoid disturbance by overlapping γ -lines from undesired sources and to evaluate the longer-lived radio-nuclides more accurately.

3. Data analysis and results

The average alpha energies of the first Nb foil in two different stacked-foils were 39.25 and 38.31 MeV, respectively. The average alpha energy of the subsequent Cu and Nb foils were also calculated by using the computer program SRIM-2003 [43]. The uncertainty of the alpha energy for each representing energy point in the stack depends on the irradiation circumstances and the position of the foil in the stack. These are due to the initial beam energy, the thickness and homogeneity of target foils, and the beam struggling. The estimated uncertainties of alpha energies are ± 0.75 and ± 1.98 MeV at 39.25 and 8.86 MeV, respectively.

The alpha beam intensity was determined from the measured γ -ray activities of $^{66,67}\text{Ga}$ produced from the $^{\text{nat}}\text{Cu}(\alpha, x)$ reaction in each Cu monitor foil. The standard $^{\text{nat}}\text{Cu}(\alpha, x)^{66,67}\text{Ga}$ monitor reaction cross-section used in the calculation was taken from the IAEA recommended monitor reaction data [42]. The beam intensities obtained from the activities of each monitor foils are nearly constant within 1–2% variation. The average beam intensity was obtained from the average intensities of all monitor foils. The use of multiple monitor foils decreases the probability of introducing unknown systematic uncertainties during an activity determination. It was also considered that the loss of alpha beam flux was very small and very hard to deduce practically. The beam intensity was considered as constant to deduce cross-sections for each foil in the stack.

The $\text{Nb}(\alpha, xn)^{93-96\text{m},\text{g}}\text{Tc}$ reaction cross-section ($\sigma(E_i)$) of the i -th sample, was determined by using the standard equation [44]:

$$\sigma(E_i) = \frac{\lambda \cdot M \cdot C(E_i)}{\varepsilon(E_\gamma) \cdot I_\gamma \cdot N \cdot \rho \cdot t \cdot \phi \cdot (1 - e^{-\lambda t_m}) \cdot e^{-\lambda t_c} \cdot (1 - e^{-\lambda t_i})}, \quad (1)$$

where λ is the decay constant (s^{-1}) related to half-life ($\lambda = \ln 2 / T_{1/2}$). $C(E_i)$ is the net counts under the photo-peak area at the i -th sample, $\varepsilon(E_\gamma)$ is the detection efficiency of the HPGe-detector, and I_γ is the γ -ray intensity. N is the Avogadro's number (6.023×10^{23}), ρ is the target material density (8.57 g/cm^3), M is the atomic weight (92.91), t is the target thickness (cm), and ϕ is the alpha beam intensity (particle s^{-1}). The parameters t_i , t_c , and t_m are the irradiation, cooling, and counting time (s), respectively. The decay data such as $T_{1/2}$ and I_γ of the produced radio-nuclides from $^{93}\text{Nb}(\alpha, x)$ processes were taken from Refs. [45,46] and are summarized in Table 1. The Q-values and threshold energies calculated on the basis of the atomic mass evaluation [47] combined with the Q-value calculator [48] are also presented in Table 1.

It can be seen from Table 1 that the γ -ray intensity of the $^{96\text{m}}\text{Tc}$ is very poor. However, it decays to $^{96\text{g}}\text{Tc}$ by internal transition (IT) with branching intensity of 98.05%. The half-lives of $^{96\text{m}}\text{Tc}$ and $^{96\text{g}}\text{Tc}$ are 51.5 min and 14.28 d, respectively. It was not possible to obtain the $\text{Nb}(\alpha, n)$ reaction cross-section of m- and g-state of ^{96}Tc separately. Thus the total $^{93}\text{Nb}(\alpha, n)^{96}\text{Tc}$ reaction cross-section within the alpha energies of 8.86 to 39.25 MeV was obtained. In the calculation of $\text{Nb}(\alpha, n)^{96}\text{Tc}$ reaction cross-section, the 1.95% $\varepsilon^+\beta^+$ decay of $^{96\text{m}}\text{Tc}$ to ^{96}Mo was ignored. In the case of $^{95\text{m},\text{g}}\text{Tc}$, the m- and g-states have the half-lives of 61 d and 20 h, respectively. The $^{95\text{m}}\text{Tc}$ decays to $^{95\text{g}}\text{Tc}$ with IT with branching intensity of 96.12%. Due to the long half-life of $^{95\text{m}}\text{Tc}$, its $\varepsilon^+\beta^+$ decay of 3.88% to ^{95}Mo has been ignored. Thus the $^{93}\text{Nb}(\alpha, 2n)$ reaction cross-section of the m- and g-state of ^{95}Tc were possible to obtain independently. In the case of $^{94\text{m},\text{g}}\text{Tc}$, the m- and g-states have the half-lives of 52 min and 293 min, respectively. The $^{94\text{m}}\text{Tc}$ decays to $^{94\text{g}}\text{Tc}$ with negligible internal transition of $< 0.1\%$ branching intensity. Thus the $^{93}\text{Nb}(\alpha, 3n)$ reaction cross-section of the m- and g-state of ^{94}Tc were also possible to obtain independently. The reaction cross-sections of $^{94\text{m}}\text{Tc}$, $^{94\text{g}}\text{Tc}$, $^{95\text{m}}\text{Tc}$, $^{95\text{g}}\text{Tc}$, and $^{96\text{m}+\text{g}}\text{Tc}$ determined

Table 1
Nuclear spectroscopic data, reaction Q-value and threshold energies of the $^{93}\text{Nb}(\alpha, xn)^{93-96}\text{Tc}$ reactions.

Nuclear reaction	Q-value (MeV)	Threshold energy (MeV)	Nuclide	Spin states J^π	Half-life	Decay mode (%)	γ -ray energy, E_γ (keV)	γ -ray abundance, I_γ (%)
$^{93}\text{Nb}(\alpha, 4n)$	-33.466	34.914	$^{93\text{m}}\text{Tc}$	$1/2^-$	43.5 min	$\varepsilon^+\beta^+$ (23.4) IT (76.6)	391.83 2644.55	58 14.2
$^{93}\text{Nb}(\alpha, 4n)$	-33.466	34.914	$^{93\text{g}}\text{Tc}$	$9/2^+$	2.75 h	$\varepsilon^+\beta^+$ (100)	1363.02 1477.13 1520.37	66 8.7 24.4
$^{93}\text{Nb}(\alpha, 3n)$	-24.843	25.917	$^{94\text{m}}\text{Tc}$	2^-	52.5 min	$\varepsilon^+\beta^+$ (100) <IT (0.1)	871.091 1522.11 1868.88	94 4.5 5.7
$^{93}\text{Nb}(\alpha, 3n)$	-24.843	25.917	$^{94\text{g}}\text{Tc}$	7^+	293 h	$\varepsilon^+\beta^+$ (100)	702.622 916.1 849.74 871.091 916.1 1592.1	99.6 7.6 95.7 100 7.6 2.25
$^{93}\text{Nb}(\alpha, 2n)$	-14.909	15.553	$^{95\text{m}}\text{Tc}$	$1/2^-$	61 d	$\varepsilon^+\beta^+$ (96.12) IT (3.88)	582.082 835.198 786.198	29.96 5.7 8.66
$^{93}\text{Nb}(\alpha, 2n)$	-14.909	15.553	$^{95\text{g}}\text{Tc}$	$9/2^+$	20 h	$\varepsilon^+\beta^+$ (100)	765.794 947.794 1073.71	93.82 1.951 3.74
$^{93}\text{Nb}(\alpha, n)$	-7.037	7.341	$^{96\text{m}}\text{Tc}$	4^+	51.5 min	$\varepsilon^+\beta^+$ (2.05) IT (98.05)	778.224 1200.231	1.9 1.08
$^{93}\text{Nb}(\alpha, n)$	-7.037	7.341	$^{96\text{g}}\text{Tc}$	7^+	14.28 d	$\varepsilon^+\beta^+$ (100)	778.224 812.58 849.929	100 82 98

*The γ -ray energies marked with bold are used in the calculation.

from the $^{93}\text{Nb}(\alpha, xn)^{94-96}\text{Tc}$ reaction with the alpha energies from threshold to 39.25 MeV were summarized in Table 2.

In the case of $^{93\text{m,g}}\text{Tc}$, the threshold energy for $^{93}\text{Nb}(\alpha, 3n)$ reaction is 34.91 MeV, which is closer to the alpha energy of 39.25 MeV of present work. Besides this, the branching ratio is 76.6% for the internal transition of the $^{93\text{m}}\text{Tc}$ to $^{93\text{g}}\text{Tc}$ [45]. Thus the cross-section of m- and g-state of ^{93}Tc from the $^{93}\text{Nb}(\alpha, 4n)$ reaction is not possible to obtain using Eq. (1). Instead of that, the isomer ratio of $^{93\text{m,g}}\text{Tc}$ was possible to be obtained only at four alpha energies using the following relation [49]

$$\text{IR} \equiv \frac{\sigma_m}{\sigma_g} = \left[\left(\frac{N_g}{N_m} \times \frac{\varepsilon_m I_{\gamma m}}{\varepsilon_g I_{\gamma g}} - \frac{P \lambda_g}{\lambda_g - \lambda_m} \right) \times \frac{A_m B_m C_m}{A_g B_g C_g} + \frac{P \lambda_m}{\lambda_g - \lambda_m} \right]^{-1}, \quad (2)$$

$$A_i = (1 - e^{-\lambda_i t_i}), \quad B_i = e^{-\lambda_i t_c}, \quad C_i = (1 - e^{-\lambda_i t_m})/\lambda_i, \quad (3)$$

where ε_i is the detection efficiency, and $I_{\gamma i}$ is the γ -ray abundance or intensity of the i ($i = m, g$) state. λ_i is the decay constant ($\ln 2/T_{1/2}$) of these states and P is the branching fraction for the

Table 2

The cross-sections of ^{94m}Tc , ^{94g}Tc , ^{95m}Tc , ^{95g}Tc and $^{96m+g}\text{Tc}$ from the $^{93}\text{Nb}(\alpha, xn)^{94-96}\text{Tc}$ reactions at various alpha energies.

Alpha energy [MeV]	^{94m}Tc [mb]	^{94g}Tc [mb]	^{95m}Tc [mb]	^{95g}Tc [mb]	^{96}Tc [mb]
8.86 ± 1.98					0.1 ± 0.02
10.26 ± 1.82					7.3 ± 0.4
12.45 ± 1.61					51.4 ± 2.6
15.58 ± 1.40				4.6 ± 0.5	689.0 ± 34.5
17.29 ± 1.30			11.0 ± 2.6	40.7 ± 2.3	784.0 ± 39.2
19.87 ± 1.19			73.8 ± 4.1	422.0 ± 21.1	601.0 ± 30.1
21.36 ± 1.14			102.0 ± 5.5	601.0 ± 30.2	429.0 ± 21.5
23.63 ± 1.06			116.0 ± 6.0	898.0 ± 44.9	180.0 ± 9.1
24.93 ± 1.02			122.0 ± 6.3	999.0 ± 50.1	128.0 ± 6.4
27.00 ± 0.97		2.3 ± 0.6	91.0 ± 4.7	1050.0 ± 52.4	74.2 ± 3.8
28.20 ± 0.93	5.0 ± 1.2	18.9 ± 1.2	105.0 ± 5.4	1080.0 ± 54.0	60.2 ± 3.1
30.10 ± 0.90	31.2 ± 3.2	147.0 ± 7.5	73.8 ± 3.8	942.0 ± 47.1	47.6 ± 2.4
31.22 ± 0.88	50.2 ± 4.5	224.0 ± 11.3	64.7 ± 3.4	849.0 ± 42.6	38.8 ± 2.0
33.00 ± 0.84	61.3 ± 5.3	454.0 ± 22.8	40.9 ± 2.2	599.0 ± 30.0	34.8 ± 1.8
34.05 ± 0.83	67.3 ± 6.3	517.0 ± 26.0	34.6 ± 1.9	514.0 ± 25.8	28.6 ± 1.5
35.71 ± 0.80	70.2 ± 6.9	659.0 ± 33.1	24.0 ± 1.4	362.0 ± 18.1	28.5 ± 1.5
36.71 ± 0.79	69.6 ± 7.2	686.0 ± 34.4	21.6 ± 1.3	300.0 ± 15.1	23.2 ± 1.2
38.71 ± 0.75	66.3 ± 7.1	760.0 ± 38.1	16.2 ± 1.0	219.0 ± 11.0	23.2 ± 1.2
39.25 ± 0.75	58.9 ± 7.2	730.0 ± 36.6	12.8 ± 0.9	188.0 ± 9.5	18.3 ± 1.0

decay of the m- to g-state. The parameters t_i , t_c , and t_m are the irradiation, cooling, and counting time (s), respectively.

The isomeric ratios of $^{93m,g}\text{Tc}$ calculated in the above method at four alpha energies from the present work are given in Table 3. From the measured cross-sections of m- and g-state of $^{94,95m,g}\text{Tc}$, their isomeric ratios were obtained and listed in Table 3. However, the IR values given in Table 3 are $\sigma_{\text{high-spin}}/\sigma_{\text{low-spin}}$ based on the cross-section for high-spin ground state to that for low-spin meta-stable state.

The errors on the isomeric ratios are the propagated error from the reaction cross-sections. The overall uncertainty of the cross-sections comes from both statistical and systematic errors. The random error in the observed activity is primarily due to counting statistics, which is estimated to be 3–8%. This can be determined by accumulating the data for an optimum time period that depends on the half-life of the nuclides of interest. On the other hand, systematic errors are those that affect all the results in the same way. The systematic errors are due to uncertainties in alpha beam intensity (~ 2 –22%), the irradiation time ($\sim 0.5\%$), the detection efficiency calibration ($\sim 3\%$), the half-life of the reaction products, and the γ -ray abundances ($\sim 2\%$). Thus the total systematic error is about ~ 4.2 –22.3%. We have tried to make the reasonable effort to minimize or eliminate systematic errors. The overall uncertainties of the cross-section measurements were in the range of 5–23%, coming from the square root of squares of the combination of a statistical error of 3–8% and a systematic error of 4–22%.

4. Discussion

The production cross-sections of ^{94m}Tc , ^{94g}Tc , ^{95m}Tc , ^{95g}Tc , and $^{96m+g}\text{Tc}$ radio-nuclides from the $^{93}\text{Nb}(\alpha, xn)^{94-96}\text{Tc}$ reactions have been determined as given in Table 2. The reaction

Table 3

The isomeric ratios of $^{93m,g}\text{Tc}$, $^{94m,g}\text{Tc}$, and $^{95m,g}\text{Tc}$ radioisotopes from the $^{93}\text{Nb}(\alpha, xn)$ reactions at various excitation energies.

Alpha energy [MeV]	Excitation energy (MeV)	Isomeric ratio ($\sigma_{\text{high-spin}}/\sigma_{\text{low-spin}}$)		
		^{93}Tc	^{94}Tc	^{95}Tc
15.58 ± 1.40	18.02			2.296 ± 0.402
17.29 ± 1.30	19.73			2.945 ± 0.523
19.87 ± 1.19	22.31			6.050 ± 0.415
21.36 ± 1.14	23.80			7.906 ± 1.029
23.63 ± 1.06	26.07			8.616 ± 1.287
24.93 ± 1.02	27.37			9.014 ± 1.269
27.00 ± 0.97	29.44		1.780 ± 0.409	10.425 ± 0.841
28.20 ± 0.93	30.64		2.789 ± 0.368	14.579 ± 1.633
30.10 ± 0.90	32.54		4.999 ± 0.468	14.297 ± 1.863
31.22 ± 0.88	33.66		5.691 ± 0.519	16.310 ± 1.563
33.00 ± 0.84	35.44		7.055 ± 0.628	17.772 ± 1.138
34.05 ± 0.83	36.49		7.030 ± 0.317	17.263 ± 2.876
35.71 ± 0.80	38.16	8.237 ± 1.048	8.764 ± 1.226	17.008 ± 1.464
36.71 ± 0.79	39.15	12.620 ± 1.521	9.429 ± 1.246	15.027 ± 2.558
38.71 ± 0.75	40.75	20.563 ± 1.693	10.562 ± 1.064	14.178 ± 2.086
39.25 ± 0.75	41.69	21.475 ± 1.907	10.296 ± 1.103	14.857 ± 1.911

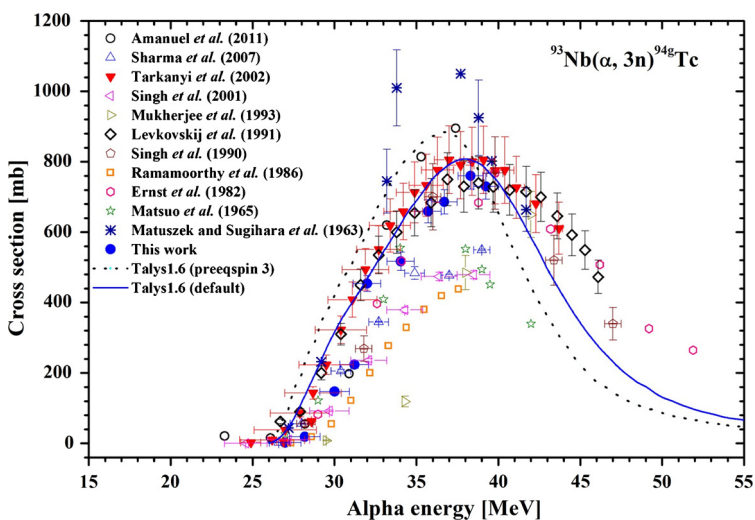


Fig. 1. The plot of experimental and TALYS $^{93}\text{Nb}(\alpha, 3n)^{94g}\text{Tc}$ reaction cross-section as a function of alpha energy.

cross-sections of ^{94g}Tc , ^{94m}Tc , ^{95g}Tc , ^{95m}Tc and total ($m + g$) of ^{96}Tc along with the available literature data [12–22] are plotted in Figs. 1–5 as a function of alpha energy. The data at higher energy from the literature are also shown in the same figures to examine the excitation function. It can be seen from Figs. 1–5 that the experimental cross-sections data of present work for ^{94g}Tc , ^{94m}Tc , ^{95g}Tc and ^{95m}Tc radio-nuclides are in agreement with the major number of literature data [11–30]. The present data for ^{96}Tc isotope are higher than those of the literature data. The cross-sections of the $^{93}\text{Nb}(\alpha, xn)^{94-96}\text{Tc}$ reactions were also calculated using the computer code TALYS 1.6 [41].

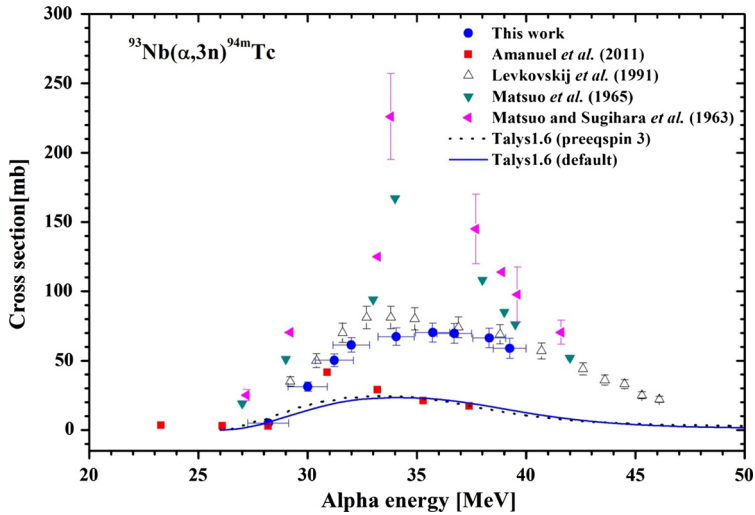


Fig. 2. The plot of experimental and TALYS $^{93}\text{Nb}(\alpha, 3n)^{94\text{m}}\text{Tc}$ reaction cross-section as a function of alpha energy.

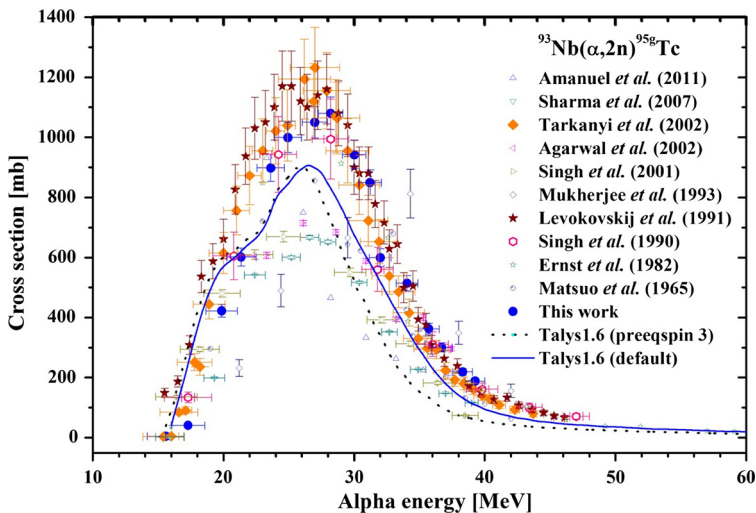


Fig. 3. The plot of experimental and TALYS $^{93}\text{Nb}(\alpha, 2n)^{95\text{g}}\text{Tc}$ reaction cross-section as a function of alpha energy.

The TALYS 1.6 program provides two options for spin distribution for the residual states after pre-equilibrium emission. The default is to adopt the compound nucleus spin distribution. Another option that has been quite often used in the past is to assign a spin distribution to the particle-hole state density. For that, we adopt the usual decomposition of the state density into an angular momentum-dependent part and an energy-dependent part. There are various arguments to prefer the compound nucleus spin distribution and thus the TALYS 1.6 code is used default parameters. Flag to use the pre-equilibrium or compound nucleus spin distribution for the pre-equilibrium, following options are possible. (a) Preeqspin n or preeqspin 1, in which the pre-equilibrium spin distribution is made equal to the relative spin-dependent population after compound nucleus emission; (b) preeqspin y or preeqspin 3, in which the pre-equilibrium spin

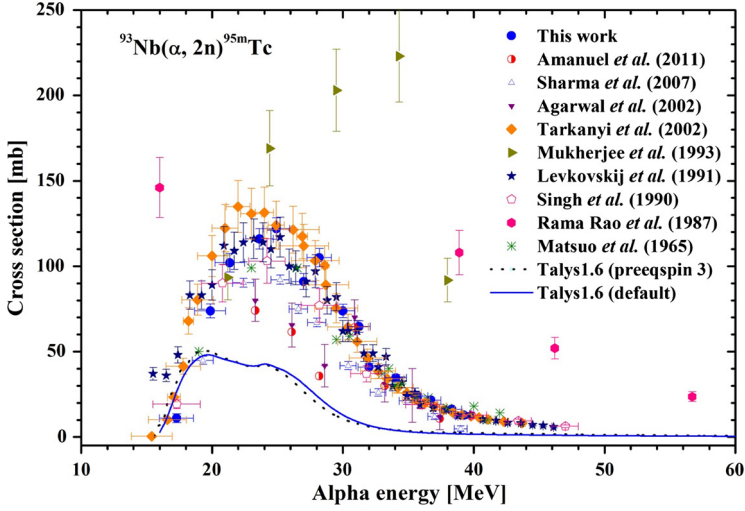


Fig. 4. The plot of experimental and TALYS $^{93}\text{Nb}(\alpha, 2n)^{95\text{m}}\text{Tc}$ reaction cross-section as a function of alpha energy.

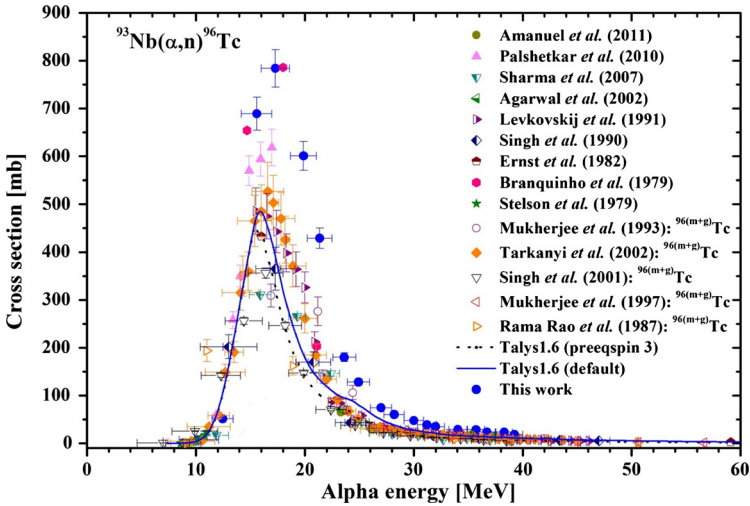


Fig. 5. The plot of experimental and TALYS $^{93}\text{Nb}(\alpha, n)^{96\text{m}+\text{g}}\text{Tc}$ reaction cross-section as a function of alpha energy.

distribution is based on particle–hole state densities. Pre-equilibrium processes cover a sizable part of the reaction cross section for incident energies between 10 ~ 200 MeV. In our measurement we have measured reactions cross section in the energy range above 10 MeV. So it is better to assign a spin distribution to the particle hole state i.e. preeqspin y or preeqspin 3. Thus we have calculated the $^{93}\text{Nb}(\alpha, xn)^{94-96}\text{Tc}$ reactions cross-sections using the computer code TALYS 1.6 [41] with default parameters and preeqspin 3 model, and are plotted in Figs. 1–5 to compare with the experimental data. The values from the TALYS 1.6 have the similar trend of the experimental data. However, the values based on preeqspin equal to 3 in the TALYS 1.6 code slightly shifted to lower energies compared to the values based on the default parameters. For the $^{93}\text{Nb}(\alpha, xn)^{94\text{g}, 95\text{g}, 96}\text{Tc}$ reaction cross-sections calculated from the TALYS 1.6 code with

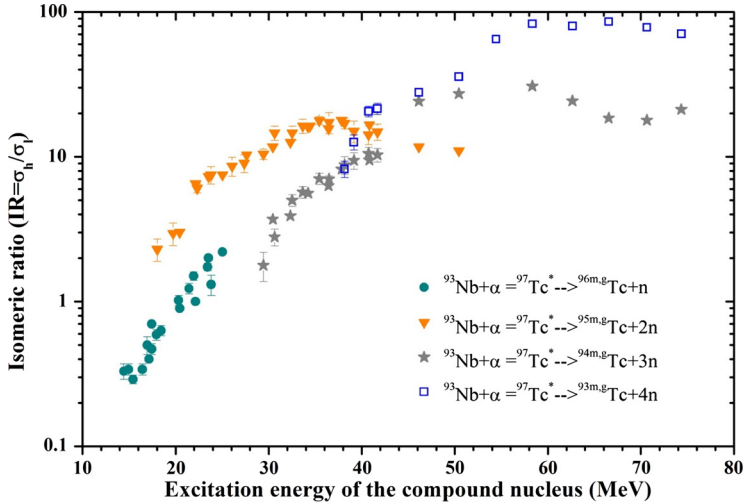


Fig. 6. The plot of isomeric cross-section ratios of $^{93m,g}\text{Tc}$, $^{94m,g}\text{Tc}$, $^{95m,g}\text{Tc}$ and $^{96m,g}\text{Tc}$ from the $^{93}\text{Nb}(\alpha, xn)$ reaction as a function of excitation energies.

default parameters were in general agreement with the experimental data of present work and literature data [11–30]. On the other hand, the reaction cross-sections of $^{93}\text{Nb}(\alpha, xn)^{94m,95m}\text{Tc}$ calculated from the TALYS 1.6 code based on both default parameters and preeqspin model with 3 are lower than those of the present work and the literature [11–30].

Thus based on the similar trend of experimental cross-sections of the present work and literature data, the isomeric ratios should be coherent. In spite of this, the isomeric ratios of ^{94}Tc , ^{95}Tc , and ^{96}Tc isomeric pairs varies from one work to others [13,15]. The isomeric ratios of ^{94}Tc , ^{95}Tc , and ^{96}Tc isomeric pairs from the $^{93}\text{Nb}(\alpha, xn)$ reactions determined by Matso et al. [13] are consistently lower than the values of Branquinho et al. [15]. Within the energy range below 40 MeV, the isomeric ratios of ^{94}Tc and ^{95}Tc from the present work are in agreement with the values of Branquinho et al. [15]. The isomeric ratios of ^{93}Tc obtained by Branquinho et al. [15] are available at higher energies. There are no isomeric ratios of the $^{93m,g}\text{Tc}$ radio-nuclide at lower energies in literature to compare with the present data.

In order to examine the trend of the isomeric ratios, the values from the present work along with the data of Branquinho et al. [15] for ^{93}Tc , ^{94}Tc , ^{95}Tc , and ^{96}Tc isomeric pairs are plotted in Fig. 6 as a function of excitation energy. The isomeric ratios of $^{96m,g}\text{Tc}$ obtained by Branquinho et al. [15] are only for few numbers of alpha energies. So the data of Matso et al. [13] for the $^{96m,g}\text{Tc}$ isomeric pairs are also plotted in the same figure for comparison and to examine the trend. It can be seen from Fig. 6 that the isomeric ratios of $^{93m,g}\text{Tc}$, $^{94m,g}\text{Tc}$, $^{95m,g}\text{Tc}$, and $^{96m,g}\text{Tc}$ isomeric pairs from the $^{93}\text{Nb}(\alpha, xn)$ reactions increase with the increasing excitation energy. This observation indicates the role of excitation energy. However, the increase trend is up to certain excitation energy where a compound nucleus phenomenon holds [27,28,40]. Once pre-equilibrium process starts [5], the isomeric ratio decreases [26–28] with increasing excitation energy. This is because in the process of compound nucleus, the low energy nucleons are evaporated isotropically from an excited nucleus in the statistical equilibrium [1,2]. However, at higher excitation energy the non-compound or pre-equilibrium process starts [5,40,50,51], in which the emission of nucleons or nucleon clusters occurs with high excitation energy pre-dominantly in the forward direction. Since the high energy particles are emitted to the forward direction in

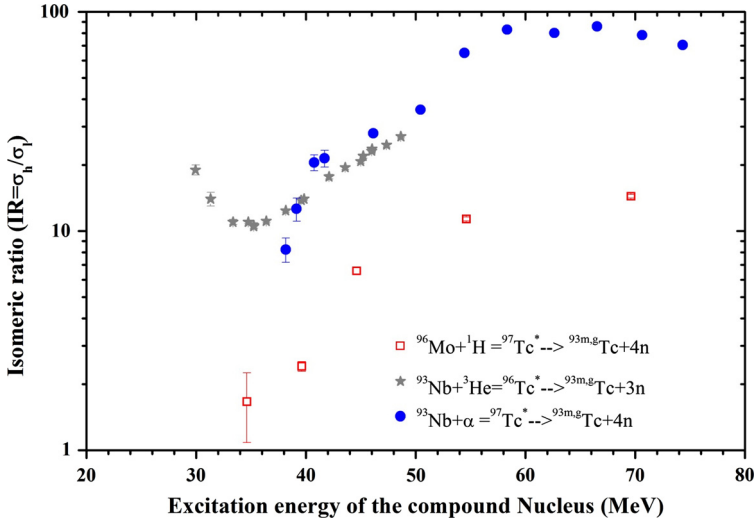


Fig. 7. The plot of isomeric cross-section ratios of $^{93m,g}\text{Tc}$ from the in $^{93}\text{Nb}(\alpha, xn)$, $^{93}\text{Nb}({}^3\text{He}, xn)$ and $^{96}\text{Mo}(p, xn)$ reactions as a function of excitation energy.

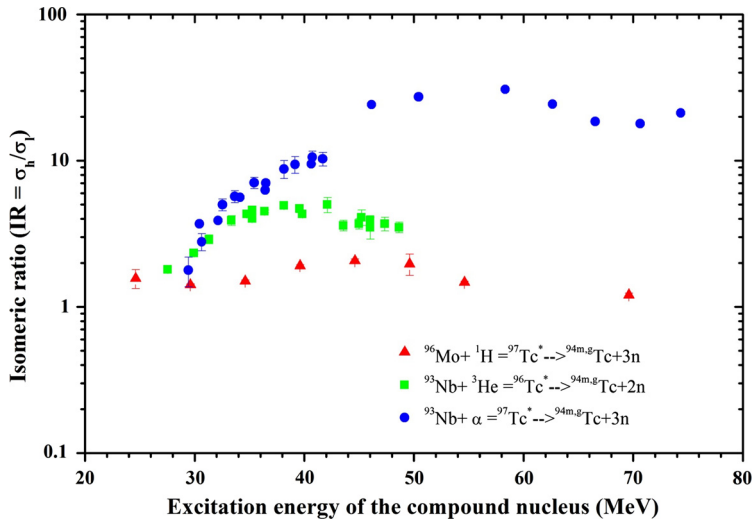


Fig. 8. The plot of isomeric cross-section ratios of $^{94m,g}\text{Tc}$ from the in $^{93}\text{Nb}(\alpha, xn)$, $^{93}\text{Nb}({}^3\text{He}, xn)$ and $^{96}\text{Mo}(p, xn)$ reactions as a function of excitation energy.

the pre-equilibrium reactions, they will remove on an average much more spin than that by the isotropically emitted particles in the compound nucleus process. The pre-equilibrium process will affect the angular momentum distribution of the residual nuclei. Thus the spin distribution of the residual nuclei is on an average less than the initial spin distribution due to the large amount of angular momentum that can be carried away by the emitted high energy particles [40,50,51].

Besides the above fact, in the process of compound nucleus and pre-equilibrium phenomena, the input angular momentum also plays its role besides excitation energy. In order to explain this,

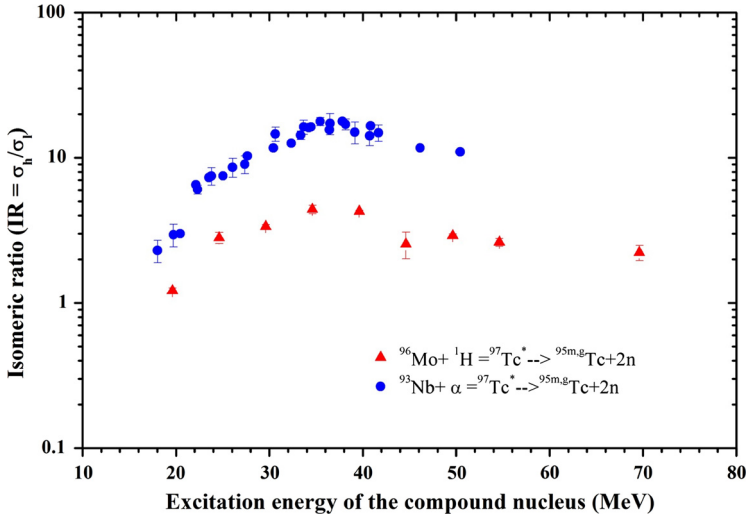


Fig. 9. The plot of isomeric cross-section ratios of $^{95m,g}\text{Tc}$ from the in $^{93}\text{Nb}(\alpha, xn)$ and $^{96}\text{Mo}(p, xn)$ reactions as a function of excitation energy.

the isomeric yield ratios of ^{93}Tc and ^{94}Tc in the $^{93}\text{Nb}(\alpha, xn)$ reaction from Table 3 as well as in the $^{93}\text{Nb}({}^3\text{He}, xn)$ [32] and $^{96}\text{Mo}(p, xn)$ [31] reactions from literature are plotted in Figs. 7 and 8 as a function of excitation energy. Similarly, the isomeric ratios of $^{95m,g}\text{Tc}$ in the $^{93}\text{Nb}(\alpha, xn)$ reactions from Table 3 and in the $^{96}\text{Mo}(p, xn)$ [31] reactions from literature are plotted in Fig. 9 as a function of excitation energy. At all excitation energy, the isomer ratios of the Tc-isotopes in the $^{93}\text{Nb}(\alpha, xn)$ and the $^{93}\text{Nb}({}^3\text{He}, xn)$ reactions are higher than those in the $^{96}\text{Mo}(p, xn)$ reactions. This indicates the effect of input angular momentum besides the role of excitation energy. From Figs. 6–9, it can be also seen that the decreasing trend of isomeric ratios due to pre-equilibrium reaction start at lowest energy for ^{96}Tc and at highest energy for ^{93}Tc . This is because the threshold energy is lowest for ^{96}Tc and highest for ^{93}Tc . Further, it can be seen from Figs. 7–9 that for the same Tc-isotope, the decreasing trend of isomeric ratio and thus the starting of pre-equilibrium reaction is not the same in the $^{93}\text{Nb}(\alpha, xn)$, $^{93}\text{Nb}({}^3\text{He}, xn)$, and $^{96}\text{Mo}(p, xn)$ reactions. As an example the isomeric ratio of $^{93m,g}\text{Tc}$ isomeric pair is comparable at lower excitation energy in between $^{93}\text{Nb}(\alpha, xn)$ and $^{93}\text{Nb}({}^3\text{He}, xn)$ reactions. Similar is the case for the isomeric ratio of $^{94m,g}\text{Tc}$ in between $^{93}\text{Nb}(\alpha, xn)$ and $^{93}\text{Nb}({}^3\text{He}, xn)$ reactions. However, the decrease trend of isomeric ratio and thus the starts of pre-equilibrium reaction takes place at lower excitation energy in the $^{93}\text{Nb}({}^3\text{He}, xn)$ reaction than in the $^{93}\text{Nb}(\alpha, xn)$ reaction (Fig. 8). These observations indicates that the starting of pre-equilibrium reaction depend on the nature of target, projectiles and ejectiles as well as the entrance channel parameters such as excitation energy, input angular momentum.

5. Conclusions

- We have measured the excitation functions for the production of $^{93-96}\text{Tc}$ radioisotopes from the $^{93}\text{Nb}(\alpha, xn)$ reactions in the alpha energy regions of 8–40 MeV by using the stacked-foil activation technique with an overall uncertainty of 5–23%. Measured data were compared with data from literature and theoretical data from the TALYS 1.6 code based on parameters

with both default and preeqspin equal to 3. The results of ^{94g}Tc , ^{95g}Tc , and ^{96}Tc radio-nuclides from the present work are in general agreement with those of literature as well as the theoretical values from the TALYS 1.6 code based on default parameters. However, the present and literature values for the excitation functions of ^{94m}Tc and ^{95m}Tc radio-nuclides are higher than those of the TALYS 1.6 code based on both default parameters and preeqspin 3 model.

- We have determined the isomeric ratios for the $^{94m,g};^{95m,g}\text{Tc}$ isomeric pairs from the $^{93}\text{Nb}(\alpha, xn)$ reaction by using the measured cross-sections. We have also compared the measured isomeric ratios for the $^{93-96}\text{Tc}$ radio-nuclides from the $^{93}\text{Nb}(\alpha, xn)$, $^{93}\text{Nb}(^3\text{He}, xn)$, and $^{96}\text{Mo}(p, xn)$ reactions from the present work as well as literature data. It shows that within the compound nucleus reaction domain, the isomeric ratios increase with the increasing excitation energy and input angular momentum. This indicates the effect of entrance channel parameters. However, at higher excitation energy, the isomeric ratios decrease when the pre-compound process starts.
- The starting of pre-equilibrium reactions is different for the different technetium isotopes for various reactions such as $^{93}\text{Nb}(\alpha, xn)$, $^{93}\text{Nb}(^3\text{He}, xn)$, and $^{96}\text{Mo}(p, xn)$ reactions. This indicates that starting of pre-equilibrium depends on the nature of target, projectiles, and ejectiles as well as the entrance channel parameters such as excitation energy and input angular momentum.

Acknowledgements

We are thankful to the staff of Variable Energy Cyclotron Centre (VECC), Kolkata, to running the cyclotron and providing the stable alpha particle beam to carry out the experiment. This research partly was supported by the National Research Foundation of Korea (NRF) through a grant provided by the Korean Ministry of Science, ICT and Future Planning (MSIP) (NRF-2013R1A2A2A01067340) and by the Institutional Activity Program of Korea Atomic Energy Research Institute.

References

- [1] J.R. Huizenga, R. Vandenbosch, *Phys. Rev.* 120 (1960) 1305.
- [2] R. Vandenbosch, J.R. Huizenga, *Phys. Rev.* 120 (1960) 1313.
- [3] R. Vandenbosch, J.R. Huizenga, *Nuclear Fission*, Academic Press, New York, 1973.
- [4] C. Wagemans, *The Nuclear Fission Process*, CRC, London, 1990.
- [5] M. Blann, *Annu. Rev. Nucl. Sci.* 25 (1975) 123.
- [6] M.B. Chadwick, et al., ENDF/B-VII.0: next generation evaluated nuclear data library for nuclear science and technology, *Nucl. Data Sheets* 107 (2006) 2931.
- [7] K. Shibata, et al., JENDL-4.0: a new library for nuclear science and engineering, *J. Nucl. Sci. Technol.* 48 (2011) 1.
- [8] A.J. Koning, et al., The JEFF evaluated data project, in: *Proceedings of the International Conference on Nuclear Data for Science and Technology*, Nice, 2007, EDP Sciences, 2008.
- [9] Z.G. Ge, et al., China Evaluated Nuclear Data Library, CENDL-3.1 (2009); The Updated Version of Chinese Evaluated Nuclear Data Library (CENDL-3.1), in: *Proceedings of the International Conference on Nuclear Data for Science and Technology*, Jeju Island, Korea, 2010.
- [10] IAEA-EXFOR Database, <http://www-nds.iaea.org/exfor>.
- [11] J.M. Matuszek, T.T. Sugihara, *Nucl. Phys.* 42 (1963) 582.
- [12] P.H. Stelson, F.K. McGowan, *Phys. Rev.* 133 (1964) B911.
- [13] T. Matsuo, J.M. Matuszek, N.D. Dudey Jr., T.T. Sugihara, *Phys. Rev.* 139 (1965) B886.
- [14] P. Bond, S. Jha, *Phys. Rev. C* 5 (1970) 1887.
- [15] C.L. Branquinho, S.M.A. Hoffmann, G.W.A. Newton, V.J. Robinson, H.-Y. Wang, I.S. Grant, J.A.B. Goodall, *J. Inorg. Nucl. Chem.* 41 (1979) 617.

- [16] J. Ernst, R. Ibowski, H. Klampfl, H. Machner, T. Mayer-Kuckuk, R. Schanz, *Z. Phys. A* 308 (1982) 301.
- [17] N. Ramamoorthy, M.K. Das, B.R. Sarkar, R.S. Mani, *J. Radioanal. Nucl. Chem.* 98 (1986) 121.
- [18] J. Rama Rao, A.V. Mohan Rao, S. Mukherjee, R. Upadhyay, N.L. Singh, S. Agarwal, L. Chaturvedi, P.P. Singh, *J. Phys. G* 13 (1987) 535.
- [19] N.L. Singh, S. Agarwal, J. Rama Rao, *J. Phys. Soc. Jpn.* 59 (1990) 3916.
- [20] V.N. Levkovskij, *Activation Cross Section by Protons and Alphas*, Moscow, 1991.
- [21] S. Mukherjee, M.H. Rashid, S.N. Chintalapudi, *Pramāna* 41 (1993) 329.
- [22] S. Mukherjee, N.L. Singh, *J. Phys. G* 22 (1996) 1455.
- [23] S. Mukherjee, N.L. Singh, A.V. Mohan Rao, L. Chaturvedi, P.P. Singh, *Phys. Scr.* 55 (1997) 409.
- [24] R.K.Y. Singh, M.A. Ansari, R.P. Gautam, *Chin. J. Phys.* 39 (2001) 336.
- [25] F. Tarkanyi, F. Ditroi, F. Szelecsenyi, M. Sonck, A. Hermanne, *Nucl. Instrum. Methods Phys. Res., Sect. B, Beam Interact. Mater. Atoms* 198 (2002) 11.
- [26] A. Agarwal, I.A. Rizvi, A.K. Chaubey, *Phys. Rev. C* 65 (2002) 034605.
- [27] S. Mukherjee, N.L. Singh, G.K. Kumar, L. Chaturvedi, *Phys. Rev. C* 72 (2005) 014609.
- [28] M.K. Sharma, H.D. Bhardwaj Unnati, Pushpendra P. Singh, B.P. Singh, R. Prasad, *Eur. Phys. J. A* 31 (2007) 43.
- [29] C.S. Palshetkar, S. Santra, A. Chatterjee, K. Ramachandran, S. Thakur, S.K. Pandit, K. Mahata, A. Shrivastava, V.V. Parkar, V. Nanal, *Phys. Rev. C* 82 (2010) 044608.
- [30] F.K. Amanuel, B. Zelalem, A.K. Chaubey, Avinash Agarwal, I.A. Rizvi, *Chin. J. Phys.* 49 (2011) 884.
- [31] J.J. Hogan, *J. Inorg. Nucl. Chem.* 35 (1973) 705.
- [32] L.T. Aiuler, A.G. Da Silva, G.W.A. Newton, *J. Inorg. Nucl. Chem.* 43 (1981) 2611.
- [33] M.C. Lagunas-Solar, P.M. Kiefer, O.F. Carvacho, C.A. Lagunas, P.C. Ya, *Radiochim. Acta* 60 (1993) 57.
- [34] S. Takacs, F. Tarkanyi, M. Sonck, A. Hermanne, *Nucl. Instrum. Methods Phys. Res., Sect. B, Beam Interact. Mater. Atoms* 198 (2002) 183.
- [35] M.S. Uddin, M. Hagiwara, F. Tarkanyi, F. Ditroi, M. Baba, *Appl. Radiat. Isot.* 60 (2004) 911.
- [36] M.U. Khandaker, A.K.M.M.H. Meaze, K. Kim, D. Son, G. Kim, Y.S. Lee, *J. Korean Phys. Soc.* 48 (2006) 821.
- [37] M.U. Khandakar, M.S. Uddin, K.S. Kim, Y.S. Lee, G.N. Kim, *Nucl. Instrum. Methods Phys. Res., Sect. B, Beam Interact. Mater. Atoms* 262 (2007) 171.
- [38] M.S. Uddin, M. Baba, *Appl. Radiat. Isot.* 66 (2008) 208.
- [39] A.A. Alharbi, J. Alzahrani, A. Azzam, *Radiochim. Acta* 99 (2011) 763.
- [40] H.H. Bissem, R. Georgi, W. Scobel, J. Ernst, M. Kaba, J. Rama Rao, H. Strohe, *Phys. Rev. C* 22 (1980) 1468.
- [41] A.J. Koning, S. Hilaire, M.C. Duijvestijn, TALYS-1.6, A nuclear reaction program, NRG-1755 NG Petten, The Netherlands, 2008, <http://www.talys.eu>.
- [42] S.M. Qaim, F. Tárkányi, P. Obložinský, K. Gul, A. Hermanne, M.G. Mustafa, F.M. Nortier, B. Scholten, Yu. Shubin, S. Takács, Y. Zhuang, Charged particle cross-section database for medical radioisotope production: diagnostic radioisotopes and monitor reactions, IAEA-TECDOC-1211, Vienna, 2001, available from <http://www-nds.iaea.org/medical/>.
- [43] J.F. Ziegler, *Nucl. Instrum. Methods Phys. Res., Sect. B, Beam Interact. Mater. Atoms* 219–220 (2004) 1027, available from <http://www.srim.org/>.
- [44] G. Gilmore, J.D. Hemingway, *Practical Gamma-Ray Spectrometry*, John Wiley and Sons, England, 1995, p. 17.
- [45] R.B. Firestone, L.P. Ekstrom, in: *Table of Radioactive Isotopes*, 2004, version 2.1, available from: <http://ie.lbl.gov/toi/index.asp/>.
- [46] National Nuclear Data Center, Brookhaven National Laboratory, Chart of Nuclide. Available from: <http://www.nndc.bnl.gov/chart>.
- [47] G. Audi, A.H. Wapstra, *Nucl. Phys. A* 595 (1995) 409.
- [48] National Nuclear Data Center, Brookhaven National Laboratory, Q-value calculator. Available from: <http://www.nndc.bnl.gov/qcalc/>.
- [49] R. Vanska, R. Rieppo, *Nucl. Instrum. Methods Phys. Res.* 179 (1981) 525.
- [50] J.M. Daugas, R. Grzywacz, M. Lewitowicz, M.J. Lopez-Jimenez, F. de Oliveira-Santos, J.C. Angeélique, L. Axelson, C. Borcea, C. Longour, G. Neyens, *Phys. Rev. C* 63 (2009) 064609.
- [51] M. Avrigeanu, V. Avrigeanu, M. Diakaki, R. Vlastou, *Phys. Rev. C* 85 (2012) 044618.